# Nonlinear Fourier analysis of deep-water, random surface waves: theoretical formulation and experimental observations of rogue waves

A. R. Osborne, M. Onorato, and M. Serio

Dipartimento di Fisica Generale dell'Università, Via Pietro Giuria 1, Torino 10125, Italy

**Abstract**. Unidirectional deep-water waves are studied theoretically and experimentally. Theoretically we apply the theory of the *nonlinear Schroedinger equation* (NLS) using the *inverse scattering transform*, a kind of generalized, *nonlinear Fourier analysis*. We discover from the theoretical study that there are essentially four kinds of physical effects that can lead to extreme waves: (1) the superposition of sine waves, (2) the Stokes wave nonlinearity, (3) the Benjamin-Feir instability and (4) the wave/current interaction. In the context of nonlinear random wave trains, item (3) is of prime interest here and we discuss how the theory predicts the existence of *unstable wave packets* which constitute a *second population* of nonlinear waves, the *first population* being the weakly nonlinear superposition of sine waves (item (1)) together with the Stokes-wave correction (item (2)). The second population, unstable wave packets, which can rise up to more than twice the significant wave height, are a *new nonlinear spectral component* in nonlinear random waves. Do second population waves actually exist in water waves? To answer this question we conducted a number of random wave experiments at Marintek, Trondheim, and assessed the results in terms of the NLS spectral theory. We find that the second population waves not only exist, but they can also, under the circumstances discussed herein, dominate the energetics of the wave train leading to a condition we call a "rogue sea." Indeed, we also find in a companion paper (Onorato, Osborne, and Serio, 2005) that the extreme events associated with the Benjamin-Feir instability can also lead to a large enhancement in the tail of the Rayleigh distribution for crest and wave heights.

## 1. Introduction

This paper addresses a new approach for the Fourier analysis of nonlinear, deep-water wave trains. The method is intrinsically nonlinear and describes a *nonlinear Fourier spectrum* for a random wave train which includes:

(1) The *superposition of weakly-nonlinear sine wave* components. This small-amplitude limit of the theory is just ordinary linear Fourier analysis.
(2) The Stokes wave nonlinearity.
(3) The nonlinear superposition of nonlinear, unstable wave packets and their space/time dynamics. This contribution arises from the Benjamin-Fier instability.
(4) The influence of the *wave/current interaction* on the nonlinear spectrum.

Items (1), (2) and (4) are well known in the study of random wave trains and we do not discuss them in detail herein, although many other authors in this proceedings volume provide overviews and appropriate perspective: (Donelan and Magnusson, Forristall, Graber, Haver, Henyey, Magnusson and Donelan, Melville, Olagnon and Prevosto). While we refer to the traditional "linear superposition of sine waves" as *first population* waves, we also include in this category the small perturbations which give rise to the Stokes wave nonlinearity (*Tayfun*, 1980; *Forristall et al*., 2000). Full nonlinear simulations have been considered by Yue and coauthors (Wu et al., this volume). Nonlinear modulations are also considered herein by Dysthe, by Segur, and by Schober. Wave breaking, beyond the scope of the pre-

sent work, is considered by Banner and by Donelan and Magnusson. Remote sensing aspects of rogue waves are considered by Lehner and by Rosenthal.

The focus in the present paper is to address *second population* waves, i.e., unstable wave packets governed by the Benjamin-Feir instability. In the nonlinear Schroedinger (NLS) theoretical formulation discussed herein, the first and second population waves are different kinds of spectral components, uniquely distinguishable from each other. In the historical context of the study of ocean waves, most time series are dominated by first population waves, but for certain particular kinds of sea states one can also have a contribution from second population waves. Indeed for sea states that we refer to as *rogue seas,* the *second population waves energetically dominate the first population waves* in the nonlinear spectrum. In this case second population waves lead to an enhanced tail in the distribution of wave and crest heights (*Onorato et a*l., this volume). Rogue seas are thus characterized by a number of extreme waves greater than anticipated in a linear sea state with Rayleigh statistics.

The NLS theoretical formulation *covers all of the physical effects* in the list above (1)-(4). Indeed the *nonlinear spectral analysis* of measured wave trains reduces to an *ordinary linear Fourier series for sufficiently small waves*. On the other hand, for sufficiently large amplitude waves, a *nonlinear threshold* is reached when the second population waves begin to appear in the nonlinear Fourier spectrum. Once this threshold is surpassed in a growing sea state a rogue sea begins to build.

It is commonly recognized that a leading causal factor for the increased modern observance of rogue waves, with respect to the historical past, is *climate change*. Indeed a recent appeal has been made in the shipping industry to include this fact for future ship design (ref). We note that the present theory is consistent with the assumption that rogue waves are climate induced. This is because climate change has presumably resulted in enhanced significant wave heights over recent years (*Graveson*, 2005). The threshold effect, in which stable first population waves are converted to second population unstable wave packets, could be partially responsible for the increased statistical occurrence of freak waves in recent years.

The focus of the present paper is to "push" the nonlinear theory beyond this threshold using the *Benjamin-Feir parameter* in order to study theoretically and experimentally random wave trains in which the second population waves dominate. Let us now look at some of the theoretical aspects of deep-water wave trains.

How is it that a nonlinear Fourier approach can simultaneously contain all of the features discussed above? One begins by writing a linear wave equation for the envelope of a linear wave train:

$$i(\psi_t + C_g\psi_x) + \mu\psi_{xx} = 0 \qquad (1)$$

where $\psi(x,t)$ is the *complex envelope* of the wave train, $C_o = d\omega_o/dk_o = \omega_o/2k_o$ is the *group speed*, $\omega_o$ is the carrier *frequency*, $k_o$ is the *wave number*, $\omega_o^2 = gk_o$ is the deep-water dispersion relation and $\mu = (1/2)d^2\omega_o/dk_o^2 = -\omega_o/8k_o^2$. Eq. (1) is just about the simplest wave equation imaginable: It includes packets that have a group speed, $C_g$, and which linearly disperse. The complex envelope function, $\psi(x,t)$, is related to the *sea surface elevation*, $\eta(x,t)$, by

$$\eta(x,t) = \frac{1}{2}\left[\psi(x,t)e^{ik_o x - i\omega_o t} + c.c.\right] \qquad (2)$$

Because (1) and (2) are linear equations, the Fourier structure is trivial: The usual linear Fourier transform solves (1) for all (Cauchy) initial conditions! So, assuming that (1) is true, then (a) modeling of wave trains is simple (the FFT algorithm suffices for computing the space/time evolution), (b) the Fourier analysis of oceanic data is also straightforward, and (c) the computation of Fourier and power spectra follows in a natural way. It is hard to imagine having a better theory than (1), (2). We have all the tools for understanding how linear waves behave in the oceanic environment. Of course (1) is narrow banded, but we can always improve this feature to arbitrary order by adding additional linear dispersive terms to the equation.

For wind-wave modeling we ordinarily go a step farther by introducing a kinetic equation, beginning with the Euler equations, which includes nonlinear three-, four- or five-wave interactions, and the results have resulted in spectacular improvement in predictive capability over the last few decades (*Komen et al*., 1994). However, wind wave models, being based on kinetic equations, filter out coherent effects in a nonlinear wave train, i.e. solitary waves, wave packet solitons and unstable packet modes (in the Benjamin-Feir sense as discussed herein) are not included, or are only partially included in kinetic equations (*Janssen*, 2003; *Cavaleri*, this volume).

Recently a number of authors have presented the case for understanding a number aspects of oceanic rogue wave dynamics through application of the Benjamin-Feir instability (*Osborne et al*. 2000; *Onorato et al*., this volume; *Dysthe et al.*, this volume). The basic idea is that one can simply modify (1) to retain some of the

nonlinear effects not present in the linear approximation and in the kinetic equation formulations. A further step in enhanced understanding of these nonlinear effects is documented herein.

To modify (1) for nonlinear effects we have carried out the *simplest possible approach.* We have added a simple cubic nonlinearity (*Zakharov*, 1967; *Whitham*, 1974):

$$i(\psi_t + C_g\psi_x) + \mu\psi_{xx} + \nu|\psi|^2\psi = 0 \qquad (3)$$

where $\nu = -\omega_o k_o^2/2$. This is the so-called *nonlinear Schroedinger (NLS) equation*, the simplest possible *nonlinear* wave equation for deep-water wave dynamics. We realize that this is just a small step toward full understanding of nonlinear wave trains, but it is an important step, because as we shall see there is much to learn.

Equation (3) has the list of surprising properties (1)-(4) given above. These properties arise as a consequence of the exact solution of (3) for periodic boundary conditions using the *inverse scattering transform*. In the last half of the twentieth century a number of important theoretical developments have been made with regard to the understanding of nonlinear wave propagation (*Ablowitz and Segur*, 1981). Of particular relevance to the present work has been the discovery of large classes of *nonlinear wave equations* whose solutions may be computed without approximation using a new technique referred to as the *inverse scattering transform (IST)*. IST may be viewed as a kind of *nonlinear Fourier analysis*, valid for fully nonlinear wave motion, which has many of the nice features that render ordinary Fourier analysis such a useful tool for the time series analysis of oceanic waves. Practical implementation of IST has been made possible by a number of theoretical advances with regard to the case for *periodic boundary conditions* in which techniques are developed for the simple exploitation of the method from physical, mathematical and numerical points of view (see *Osborne* (1995, 2002) and cited references). The approach has been cast in terms of a kind of *nonlinear Fourier analysis* which, in the small amplitude limit, reduces to the ordinary, linear Fourier transform. This is only one of the reasons that the nonlinear Fourier approach may be viewed as a generalization of linear Fourier analysis.

The remainder of the paper is organized as follows. Section 2 discusses linear Fourier analysis while Section 3 discusses nonlinear Fourier analysis for the NLS equation. Section 4 discusses modulation theory for the NLS equation and provides a basis for a nonlinearity (Benjamin-Feir) parameter based on inverse scattering theory. Section 5 gives three examples of unstable wave packets. Characteristics of random wave trains subjected to the BF instability are briefly reviewed in Section 6. Section 7 discusses application of periodic inverse scattering theory to the analysis of random waves in the wave tank facility at Marintek, Trondheim, Norway.

## 2. Linear Fourier analysis

Fourier analysis allows the construction of linear wave trains, $\eta(x,t)$, by a linear superposition of sine waves:

$$\eta(x,t) = \sum_{n=1}^{N} C_n \cos(k_n x - \omega_n t + \phi_n) \qquad (4)$$

In the present case there are $N$ sine waves which are interpreted as "degrees of freedom" or "Fourier components" in the wave train. In Eq. (4) the $C_n$ are the Fourier amplitudes, the $k_n$ are the wave numbers, the $\omega_n$ are the frequencies and the $\phi_n$ are the phases. The relationship between the frequencies, $\omega_n$, and the wave numbers, $k_n$, is given by the dispersion relation, written symbolically: $\omega_n = \omega_n(k_n)$. The dispersion relation defines the physics via the correspondences

$$\frac{\partial}{\partial t} \leftrightarrow -i\omega, \qquad \frac{\partial}{\partial x} \leftrightarrow i$$

*For example the simple dispersion relation for deep water wave trains is given by*

$$\omega = C_g k + \mu k^2 \qquad (5)$$

which has the associated envelope partial differential equation (1). The simplest periodic solution to (1) is a traveling sine wave

$$\eta(x,t) = C_o \cos(k_o x - \omega_o t + \phi_o)$$

from which the general Fourier solution for $N$ components may be constructed by (4). The important point is that the *amplitudes of the sine waves and their phases are constants of the motion*, *provided that the motion is linear*. In oceanic applications one is often interested in the analysis of time series, i.e. measurements of the wave amplitude, $\eta(0,t)$, taken at a fixed spatial location over some convenient time interval; this implies setting $x = 0$ in (4).

## 3. Nonlinear Fourier analysis

We proceed by writing the NLS equation in a form that is simpler for theoretical calculations

$$iu_t + u_{xx} + 2|u|^2 u = 0 \qquad (6)$$

This equation arises from (3) by a simple rescaling and translation:

$$u = \lambda\psi\,;\; x - C_g t \to x\,;\; \mu t \to t \tag{7}$$

The Fourier structure of the nonlinear Schroedinger equation (6) is given by (Tracy and Chen, 1988).

$$u(x,t) = A_o \frac{\theta(x,t\,|\,\mathbf{B},\delta^-)}{\theta(x,t\,|\,\mathbf{B},\delta^+)} e^{2iA_o^2 t} \tag{8}$$

where the Riemann theta functions, $\theta(x,t\,|\,\mathbf{B},\delta^{\pm})$, are given by:

$$\theta(x,t) = \sum_{M_1=-\infty}^{\infty} \sum_{M_2=-\infty}^{\infty} \ldots \sum_{M_N=-\infty}^{\infty} \exp\left[ i\sum_{n=1}^{N} M_n X_n + \frac{1}{2}\sum_{m=1}^{N}\sum_{n=1}^{N} M_m B_{mn} M_n \right] \tag{9}$$

where

$$X_n = k_n x - \omega_n t - \delta_n^{\pm}$$

The wave numbers, $k_n$, frequencies, $\omega_n$, and phases, $\delta_n$, are computed by the methods of algebraic geometry (see (Osborne, 2002) for a review and a list of references). It should be noted that the theta functions (9) are just generalized Fourier series, where the *spectral amplitudes* correspond to a (Riemann) *matrix*, $\mathbf{B}$, rather than to a *vector*, $C_n$, as in linear Fourier analysis (4).

To better understand the solutions of (3) using the nonlinear Fourier decomposition (9) we consider a number of simple examples in this paper. The first example addresses the fact that the ratio of theta functions, $\theta(x,t\,|\,\mathbf{B},\delta^-)/\,\theta(x,t\,|\,\mathbf{B},\delta^+)$, is the *complex modulation envelope function*. When there is no modulation, $\theta(x,t\,|\,\mathbf{B},\delta^-)/\,\theta(x,t\,|\,\mathbf{B},\delta^+) = 1$, we have

$$u(x,t) = A_o e^{2iA_o^2 t} \tag{10}$$

This is the so-called *plane wave solution of the NLS equation*. It corresponds to an unmodulated carrier wave.

To understand the nonlinear spectral solutions of NLS it is necessary to discuss the so-called *spectral eigenvalue problem* for the NLS equation, first found by Zakharov and Shabat (1972):

$$\begin{aligned} i\phi_{1x} + iu(x,0)\phi_2 &= \lambda\phi_1 \\ -i\phi_{2x} + iu^*(x,0)\phi_1 &= \lambda\phi_2 \end{aligned} \tag{11}$$

The values of the eigenvalues, $\lambda$, are crucial for describing the solutions (8) of NLS (6). The Cauchy initial condition, $u(x,0)$, is the *potential function* in (11). Here we assume periodic boundary conditions to determine solutions of (11). Indeed one works in the $\lambda$-plane, Figure 1.

The *lambda plane* is a complex plane for the eigenvalues of (11); they have real and imaginary parts, $\lambda = \lambda_R + i\lambda_I$, corresponding to the real and imaginary axes in Figure 1. The simplest case is for the plane wave solution (10). This is the case of an unmodulated carrier wave of amplitude $A_o$. In the lambda plane (for which the spectrum is a perfect mirror image between the upper and lower half planes) the eigenvalues $\lambda = \pm iA_o$ on the imaginary axis correspond to the carrier wave, $A_o$. The modulations correspond to *double points* (pairs of eigenvalues) connected by *spines* (curves of spectrum connecting the double points). Two kinds of spectrum exist for NLS: (1) *Stokes waves* (for which the two eigenvalues of the double point are connected by a spine across the real axis) and (2) *unstable wave packets* (for which the two eigenvalues are connected by a spine contained entirely in the upper half plane (and also in the lower half plane by specular reflection). The Stokes waves have a Riemann matrix which is 1x1 (a scalar) while the unstable wave packets have a 2x2 matrix.

Unstable wave packets are characterized by double points in the upper and lower half planes. Their spectrum contains five numbers: $\{A_o, \varepsilon, \theta, \lambda_{Rc}, \lambda_{Ic}\}$ (see Figure 1). Here $A_o$ is the carrier amplitude, $\varepsilon$ is the half-distance between the double points, $\theta$ is the angle of a straight line connecting the double points and the complex pair $(\lambda_{cR}, \lambda_{cI})$ corresponds to the centroid of the double points in the lambda plane. Thus five parameters are required to describe a single unstable wave packet, i.e. the nonlinear interaction between the carrier and a long-wave unstable modulation. The unstable packet modes have very interesting physical behavior: They are packets which can, early in their evolution, correspond to a small modulation of the carrier and then later become large modulations which can reach up to several times the carrier amplitude. An important property of an unstable packet mode is the maximum amplitude it can reach during its evolution. This can be computed by the simple formula (see Figure 3 for definition of variables):

$$\frac{\eta_{\max}}{A_o} = 2\frac{\lambda_I}{A_o} + 1 \tag{12}$$

We discuss this result in more detail in the next section.

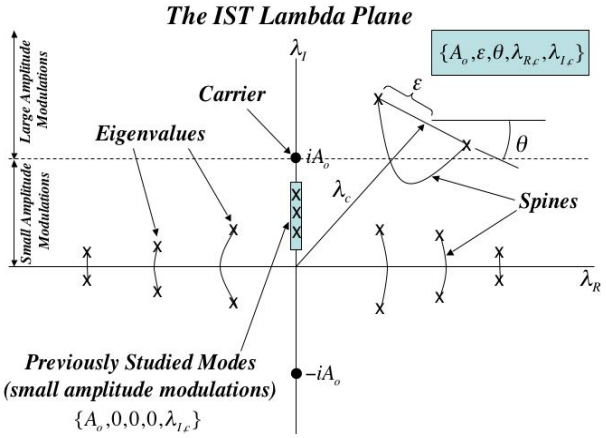


**Figure 1**. Lambda plane where the nonlinear Fourier spectrum for the NLS equation lives.

In the light of this discussion of the lambda plane it is interesting to notice where historical wave tank experiments reside in the lambda plane. Roughly, these correspond to the small vertical box of eigenvalue pairs on or near the imaginary axis as shown in Figure 1; these correspond to three of the five parameters being identically zero: $\{A_o, 0, 0, 0, \lambda_{Ic}\}$. Indeed, based on this observation, most of the lambda plane has yet to be explored. In our view, many surprises await future exploration of the entire plane.

We already know about Stokes wave solutions of the NLS equation, i.e. they correspond to the dnoidal wave solutions of the equation and are double points with spines crossing the real axis (Figure 1). To save space we move immediately to solutions of NLS that correspond to *unstable wave packets*.

## 4. Modulation theory for the NLS equation

*Small amplitude modulation theory* for the NLS equation predicts a number of interesting features about the nonlinear propagation of initially small amplitude sine wave modulations. One of the most important is shown in Figure 2 where a small amplitude modulation of a carrier wave is shown (both the real and the imaginary parts of the carrier are given). At a later time this small modulation develops into an unstable wave packet as seen in Figure 3. In the present case the maximum amplitude is about 2.6 times the carrier height.

*Growth rate*

One of the important properties of an unstable wave packet is the growth rate:

$$\Omega = i\omega_o k_o^2 a_o^2 \left(\frac{K}{2\sqrt{2}k_o^2 a_o}\right)\sqrt{1-\left(\frac{K}{2\sqrt{2}k_o^2 a_o}\right)^2} \qquad (13)$$

This is Yuen's famous result when squared, but we leave this equation in the above form to emphasize the dependence on the Benjamin-Feir parameter. The above equation is just the imaginary part of the modulation frequency and is graphed in Figure 4.

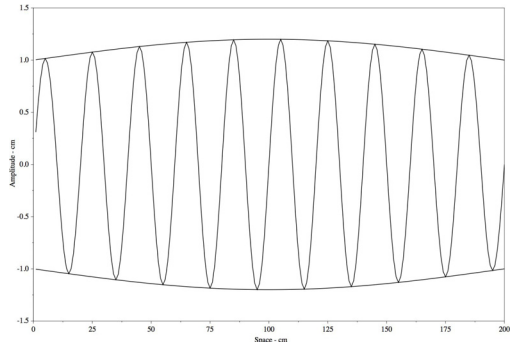


**Figure 2**. Small amplitude initial modulation of a carrier wave.

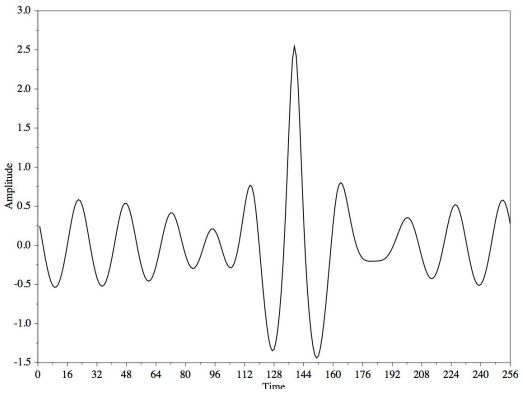


**Figure 3**. Small amplitude initial modulation of Figure 2 has grown into an unstable wave packet.

Another important property of unstable wave packets is the maximum amplitude of the packet with respect to the carrier amplitude:

$$\frac{a_{\max}}{a_o} = 1 + 2\frac{\lambda_I}{a_o} = 1 + 2\sqrt{1-\left(\frac{K}{2\sqrt{2}k_o^2 a_o}\right)^2} \qquad (14)$$

This function is graphed in Figure 5. We see that the maximum growth rate of Figure 4 (dimensionless wave number 1) is associated with an unstable wave packet that reaches a height of ~2.414 times the carrier height. Smaller modulation wave numbers are necessary to get larger packet amplitudes (up to a maximum of 3 times the carrier height), although they will take longer to reach their maximum height because the growth rate is smaller (Figure 5). However the maximum height of 3 occurs only for infinitesimal wave number.

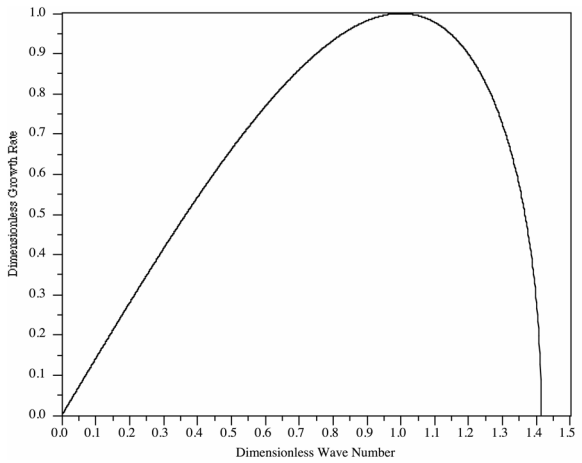


**Figure 4**. Instability diagram for small amplitude modulations for the NLS equation.

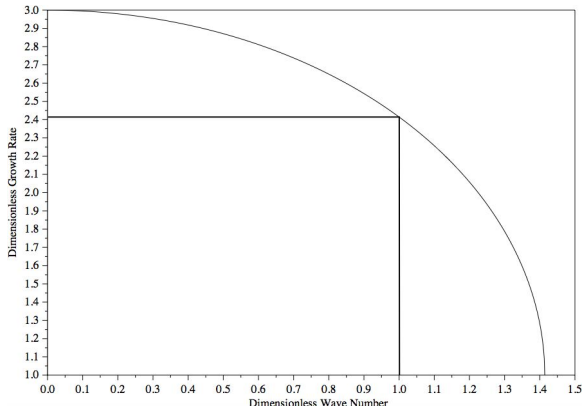


**Figure 5.** Maximum amplitude of an unstable wave packet as a function of dimensionless wave number. The maximum amplitude for the maximum growth rate (see Figure 4) is shown; the maximum amplitude is ~2.414 (see example in Figure 3).

We can also compute the imaginary part of the IST eigenvalue by the simple relation (here, as with the examples above, we assume they lie on the imaginary axis):

$$\frac{\lambda_I}{a_o} = \sqrt{1-\left(\frac{K}{2\sqrt{2}k_o^2 a_o}\right)^2}$$

As before we see that when the eigenvalue is near, but below the carrier in the lambda plane the ratio $\lambda_I / a_o \sim 1$ and hence the modulation wave number must be small and the modulation wavelength must be long.

*Time interval for rogue wave to rise to its maximum*

Another parameter that is very useful is the actual *time to appearance of an unstable mode*. Beginning with the initial small-amplitude modulation we see that this time scale can be computed by noting that:

$$\varepsilon e^{\gamma t} \sim O(1)$$

where $\varepsilon$ is the initial modulation amplitude and $\gamma$ is the imaginary part of the IST wave number (16):

$$\gamma = \omega_o k_o^2 a_o^2 \left(\frac{K}{2\sqrt{2}k_o^2 a_o}\right)\sqrt{1-\left(\frac{K}{2\sqrt{2}k_o^2 a_o}\right)^2}$$

This gives the time from the initial modulation to the maximum of an unstable mode:

$$T_* \approx |\ln \varepsilon| / \gamma$$

This is a very useful formula for determining how long it takes for a small amplitude modulation to develop into a rogue wave.

*Dissipation*

Likewise it is useful to determine if dissipation is important in wave propagation problems where rogue modes are present. Will a rogue mode come up before the waves are dissipated? For example, for linear, dissipated waves we have the approximation (*Segur*, this volume):

$$\varepsilon e^{\delta t} \sim O(1)$$

so that the waves are dissipated in the time:

$$T_{diss} \approx |\ln \varepsilon| / \delta$$

Rogue waves can be expected if $T_* << T_{diss}$, which is typically true in the ocean where $T_* \sim$ minutes and $T_{diss} \sim$ tens of hours.

*Benjamin-Feir parameter*

Periodic inverse scattering theory (*Kotljarov and Its*, 1976; *Tracy and Chen,* 1988) tells us that unstable wave packets associated with small-amplitude modulations exist when $\rho a_o L > n\pi$ where $\rho = \sqrt{2}k_o^2$ and $L > 2\pi/K$ where $K$ is the modulation wave number, $a_o$ is the carrier amplitude and $k_o$ is the carrier wave number. Here $n$ is an integer, $n = 1, 2...$ that counts the number of *unstable wave packets in a wave train*. This provides a useful definition of nonlinearity in terms of a kind of *Benjamin-Feir parameter*:

$$I_{BF} = \frac{\rho a_o L}{\pi} = \frac{2\sqrt{2}k_o^2 a_o}{K} > n \qquad (15)$$

Another useful form is obtained by noting that the number of carrier oscillations in a space series, $N_x$, below

the modulation envelope can be written $N_x = \frac{k_o}{K} = \frac{L}{L_o}$ so that the BF parameter is then

$$I_{BF} = 2\sqrt{2} N_x k_o a_o > n$$

Thus the nonlinearity is increased by increasing the steepness, $k_o a_o$ , and/or the number of carrier oscillations, $N_x$ , under the modulation envelope in a space series.

We see that $I_{BF}$ is the same parameter that appears in the growth rate (16) and the maximum amplitude (17) of an unstable packet, which we now rewrite:

$$\Omega = i\omega_o k_o^2 a_o^2 \frac{\sqrt{I_{BF}^2 - 1}}{I_{BF}^2} \tag{16}$$

$$\frac{a_{\max}}{a_o} = 1 + 2\frac{\sqrt{I_{BF}^2 - 1}}{I_{BF}} \tag{17}$$

Two of the most useful results for estimating unstable wave packet behavior can be written in terms of the Benjamin-Feir parameter!

It is also clear that an unstable wave packet (a nonlinear mode in the spectrum) has the imaginary part of the centroid of the associated double point that is also a function of the Benjamin-Feir parameter:

$$\lambda_I = a_o \frac{\sqrt{I_{BF}^2 - 1}}{I_{BF}}$$

where the inverse is given by:

$$I_{BF} = \frac{a_o}{\sqrt{a_o^2 - \lambda_I^2}}$$

Thus there is a unique relationship between the BF parameter and the spectrum of an unstable wave packet.

Note that the Benjamin-Feir parameter used herein, based upon inverse scattering theory, differs from that used in *Janssen* (2003) by an overall scale factor. The advantage of the definition used herein is that one obtains an estimate of the number of unstable modes in a time series.

## 5. Analytical formulas for some unstable wave packets

A large number of examples of unstable wave packets are known (see for example (*Osborne et al*., 2000) and cited references). We consider three cases: (1) $\{A_o, 0, 0, 0, A_o/\sqrt{2}\}$, (2) $\{A_o, 0, 0, 0, A_o\}$ and (3) $\{A_o, 0, 0, 0, \sqrt{2}A_o\}$. The first case lies on the imaginary axis below the carrier, the second lies directly on the carrier and the third lies above the carrier in the lambda plane. The first case considered has the following solution to the NLS equation:

$$u(x,t) = A_o\left[\frac{\cos[\sqrt{2}A_o x]\mathrm{sech}[2A_o^2 t] + i\sqrt{2}\tanh[2A_o^2 t]}{\sqrt{2} - \cos[\sqrt{2}A_o x]\mathrm{sech}[2A_o^2 t]}\right] e^{2iA_o^2 t} \tag{18}$$

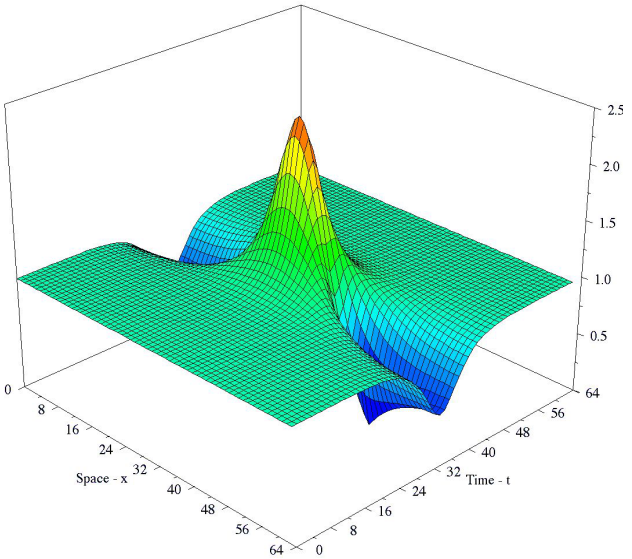


**Figure 6.** Modulus $|u(x,t)|$ of unstable wave packet that lies below the carrier in the complex lambda plane with spectrum: $\{A_0, 0, 0, 0, A_0/\sqrt{2}\}$.

The imaginary part of the eigenvalue is $\lambda_I = -iA_0/\sqrt{2}$ and the maximum packet amplitude is then given by

$$\frac{\eta_{\max}}{A_o} = 2\frac{\lambda_I}{A_o} + 1 \cong 2.414$$

This case is typical of previous studies of the Benjamin-Feir instability, i.e., a small-amplitude modulation in the far past evolves into an extreme wave event in the present. As seen in Figure 6 the small modulation is not easily visible at early times, it appears to be a broad flat plane over all $x$ at small $t$. Then exponential growth is seen to lead to a finite amplitude of ~2.41 times the carrier amplitude and then the wave decreases in amplitude as the modulation effectively disappears for large times. This solution to NLS (13) is periodic in $x$ and decays exponentially for large past and future times; it can be viewed as a single nonlinear mode (a single Fourier component) of NLS with a 2×2 period matrix.

The second case (which lies directly on the carrier) is shown in Figure 7. It has the exact solution (see *Osborne et al.*, 2000) and references therein) given by

$$u(x,t) = A_o\left[1 - \frac{4(1+4iA_o^2 t)}{1+16A_o^4 t^2 + 4A_o^2 x^2}\right] \qquad (19)$$

Here the imaginary part of the eigenvalue is $\lambda_I = iA_o$ and thus the maximum wave height is given by:

$$\frac{\eta_{\max}}{A_o} = 2\frac{\lambda_I}{A_o} + 1 = 3.0$$

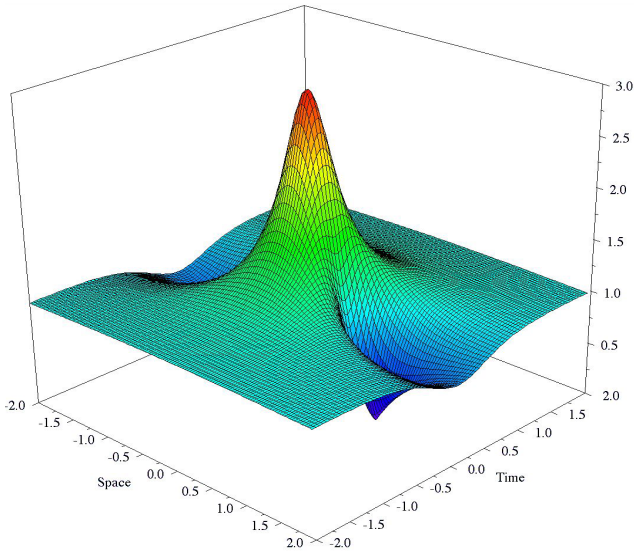


**Figure 7.** Modulus $|u(x,t)|$ of unstable wave packet that lies on the carrier in the complex lambda plane with spectrum: $\{A_o, 0, 0, 0, A_o\}$.

From (14) we see that this solution to NLS is characterized by an algebraic decay for large $x$ and $t$. In the spirit of the periodic inverse scattering transform (14) is a nonlinear Fourier component in the theory.

The third case (above the carrier) is shown in Figure 8.

$$u(x,t) = A_o\left[1 + \frac{2\left(\cos[4\sqrt{2}A_o^2 t] + i\sqrt{2}\sin[4\sqrt{2}A_o^2 t]\right)}{\cos[4\sqrt{2}A_o^2 t] + \sqrt{2}\cosh[2A_o x]}\right]e^{2iA_o^2 t} \qquad (20)$$

The eigenvalue is given by $\lambda_I = i\sqrt{2}A_o$ so that the maximum height has the value

$$\frac{\eta_{\max}}{A} = 2\frac{\lambda_I}{A} + 1 \cong 3.828$$

This case lies *above the carrier* and is no longer a small amplitude modulation for times far in the past. Indeed the solution is periodic in $t$ and exponentially decaying in $x$. Note that for small time in Figure 8 the spatial variation in the solution is a *large amplitude modulation*. This behavior is characteristic of spectral components with centroid above the carrier in the lambda plane (*Osborne*, 2002).

At this point it seems clear that there are an infinite number of solutions of the NLS equation each corresponding to particular values for the parameters in the spectrum $\{A_o, \varepsilon, \theta, \lambda_{Rc}, \lambda_{Ic}\}$. This is also true of the linear Fourier spectrum where there is a four-parameter family for amplitude $A$, wave number $k$, frequency $\omega$ and phase $\phi$ for each sine wave component: $\{A, k, \omega, \phi\}$. However, for the IST solution of the NLS equation the basis functions and the space/time dynamics are much less boring than simple sine waves, as verified in part by Figures 6-8.

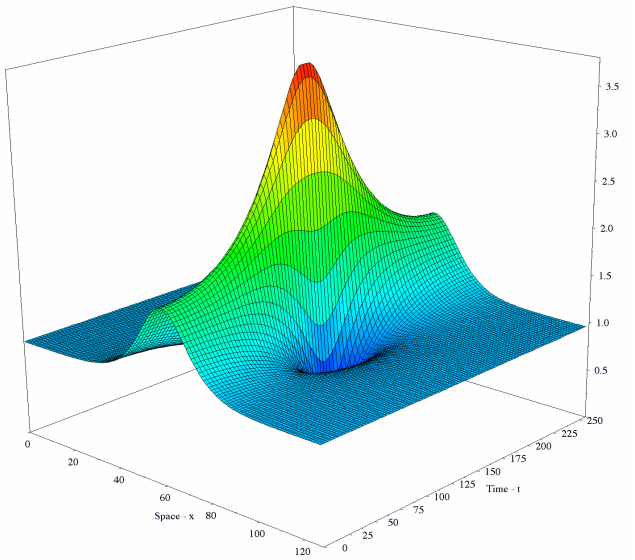


**Figure 8.** Modulus $|u(x,t)|$ of unstable wave packet that lies above the carrier in the complex lambda plane with spectrum: $\{A_o, 0, 0, 0, \sqrt{2}A_o\}$.

## 6. Characteristics of random wave trains using IST

Random wave trains from the point of view of the inverse scattering transform arise when the phases $\delta_n^{\pm}$ in (9) are taken to be uniformly distributed random numbers. Each set of dual phases $\delta_n^{\pm}$ leads to a single realization for a surface wave train governed by the nonlinear Fourier representation (8). What are some of

the properties of wave trains governed by this formulation? We now discuss a few.

We focus on a time series of length *T,* significant wave height $H_s = 4\sigma$ ($\sigma$ is the standard deviation of the time series) and $f_o$ is the peak spectral frequency. Use the fact that $\Delta k / k_o = 2\Delta f / f_o$ (where $\Delta f = 1/T$, $\Delta k \equiv K$) and the Benjamin-Feir parameter becomes:

$$I_{BF} = \sqrt{2}\,\frac{k_o a_o}{\Delta f / f_o} > n \sim \frac{\text{Carrier wave steepness}}{\text{Spectral bandwidth}}$$

or in terms of the number of carrier oscillations under the modulation, $N_t$:

$$H_{\max} = \frac{\sqrt{2}}{2}\left(2\frac{\lambda_I}{a_0} + 1\right) H_2$$

$$I_{BF} = \sqrt{2} N_t k_o a_o > n$$

(Number carrier oscillations)(steepness)

where the number of carrier oscillations in a time series is half that in a space series:

$$N_t = \frac{f_o}{\Delta f} = \frac{T}{T_o} = \frac{1}{2} N_x$$

It is common to take the *characteristic wave steepness* in a random wave train in the form:

$$k_o a_o = \frac{\sqrt{2}\pi^2}{g} H_s T_o^{-2} = \frac{\sqrt{2}\pi^2}{g} H_s f_o^2$$

where we have used $a_o = \sqrt{2}\sigma$. This definition is convenient because for a sine wave of amplitude *a* we have $\sigma = \sqrt{2}a/2$ and hence an estimate of the carrier amplitude gives the obvious result $a_o = \sqrt{2}\sigma = a$. We are left with an estimate of the Benjamin-Feir parameter for a random wave train:

$$I_{BF} = \frac{2\pi^2}{g}\frac{H_s f_o^3}{\Delta f} > n \qquad (21)$$

This provides a convenient way to estimate the number of unstable wave packets in a time series. It should be remembered that this is just a rough count of the number of unstable wave packets. Only the precise inverse scattering transform calculation will provide the optimal estimate. Figure 9 shows some of the important aspects of a time series (or space series) and its spectrum. This example is a JONSWAP power spectrum with $\gamma = 6$. It is easy to see why enhancing $\gamma$ increases the Benjamin-Feir parameter and therefore increases the number of unstable packets in a wave train. This occurs because enhancing $\gamma$ increases the steepness and decreases the bandwidth of the spectrum.

How high can unstable wave packets become with respect to significant wave height? Using $a_o = \sqrt{2}\sigma$, $H_s = 4\sigma$ and (17) we find:

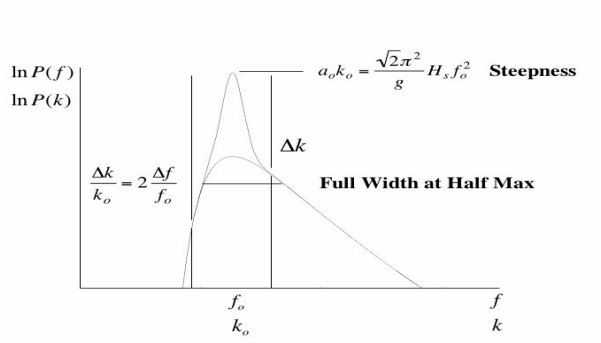


**Figure 9a.** A JONSWAP power spectrum with enhancement parameter $\gamma = 6$. Shown are the necessary parameters for computing the Benjamin-Feir nonlinearity parameter: $I_{BF} = (2\pi^2/g) H_s f_o^3 / \Delta f$.

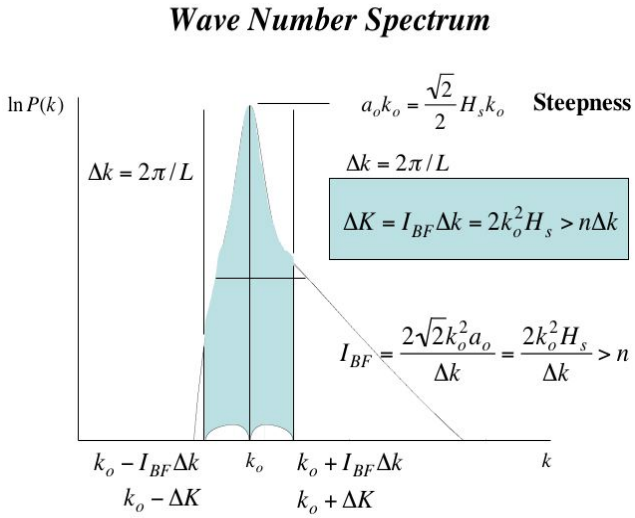


**Figure 9b**. A JONSWAP *wave number* power spectrum with enhancement parameter $\gamma = 6$. Shown is the band of wave numbers, $k_o \pm \Delta K$, about the peak wave number, $k_o$, for which instable wave packets can occur. The half-width of this band is related to the BF parameter by: $\Delta K = I_{BF}\Delta k = 2k_o^2 H_s > n\Delta k$. Here $n\Delta k$ means that $2n\Delta k$ wave number intervals about the peak are unstable. Here $I_{BF} = 2k_o^2 H_s / \Delta k > n$.

$$H_{\max} = \frac{\sqrt{2}}{2}\left(2\frac{\lambda_I}{a_o} + 1\right) H_s$$

For example,

How high can unstable wave packets become with respect to significant wave height? Using $a_o = \sqrt{2}\sigma$, $H_s = 4\sigma$ and (17) we find:

$$H_{\max} = \frac{\sqrt{2}}{2}\left(2\frac{\lambda_I}{a_o} + 1\right) H_s$$

For example. for $\lambda_I = a_o/\sqrt{2}$ we have $H_{\max} = 1.704 H_s$, for $\lambda_I = a_o$ we get $H_{\max} = 2.121 H_s$ and for $\lambda_I = \sqrt{2} a_o$ then $H_{\max} = 2.707 H_s$. These may be compared to an often-assumed "definition" of a rogue wave: $H_{\max} > 2H_s$.

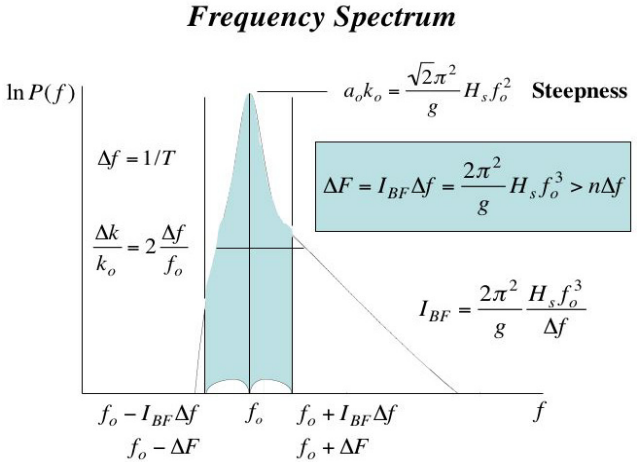


**Figure 9c**. A JONSWAP *frequency* power spectrum with enhancement parameter $\gamma = 6$. Shown is the band of frequencies, $f_o \pm \Delta F$, about the peak frequency, $f_o$, for which instable wave packets can occur. The half-width of this band is related to the BF parameter by: $\Delta F = I_{BF}\Delta f = 2\pi^2 H_s f_o^3 / g > n\Delta f$. Here $n\Delta f$ means that $2n\Delta f$ wave number intervals about the peak are unstable. Here $I_{BF} = 2\pi^2 H_s f_o^3 / g\Delta f > n$.

## 7. Trondheim wave tank experiments

We have conducted a number of deep-water, random wave experiments in the facility at Marintek in Trondheim, Norway. The tank is 10 m × 10 m × 270 m. We conducted the experiments discussed herein using standard software for wave generation using random Fourier phases and the JONSWAP power spectrum:

$$P(f) = \frac{g^2 \alpha^*}{(2\pi)^4 f^5} e^{-\frac{5}{4}\left(\frac{f_d^*}{f}\right)^4} \gamma^{\exp\left[-\frac{1}{2}\left(\left(f - f_d^*\right)/\sigma_o f_d^*\right)^2\right]}$$

For present purposes we varied only the parameter $\gamma$, the others remained their standard values. Nineteen probes were place along the tank and time series of one half hour were recorded at a rate of 40 Hz. A typical experiment is shown in Figure 10, where we used $\gamma = 6$.

The lowest time series in Figure 10 corresponds to the input JONSWAP spectrum after it had traveled for 10 m (Probe 1). Probe 8, which is herein fully analyzed for unstable wave packet behavior, is 70 m from the wave maker (count probe numbers upwards skipping the horizontal straight line above Probe 1).

The time series considered herein are shown in Figures 11 and 12; they have 4096 points and their temporal period is 102.4 s. For reference we put several properties of the wave train directly on Figures 11 and 12. The time series in Figure 11 is at Probe 1, where the properties of the waves are still quite like those expected of the JONSWAP spectrum. On the other hand Figure 12 shows the same part of the wave dynamics (found by shifting along the time axis using the linear group speed) at Probe 8, 70 meters from the wave maker. It is clear that the character of the wave train at Probe 8 is quite different from that at Probe 1. The packets at Probe 1 are broad and low, while the packets at probe 8 are narrow and high. This is the effect of the Benjamin-Feir instability on the nonlinear dynamics of a random wave train. Figure 10 offers hours of entertainment for those interested in learning how this instability affects random wave trains.

We show the linear Fourier transform of the Probe 8 time series in Figure 13. Also shown are the bounds of the band pass filter used to remove the Stokes contribution to the wave dynamics. This is a necessary step, because the NLS equation does not contain directly the Stokes effect, which is instead included only in Eq. (2).

The filtered wave train is shown in Figure 14, along with the modulus of the envelope of the wave train, which has been computed using the Hilbert transform. The standard deviation $\sigma$ of the wave train and the amplitude of the carrier wave $a_o = \sqrt{2}\sigma$ are shown in the figure.

In Figure 15 we show the results of the inverse scattering transform computation on the time series of Figure 14. We discuss briefly how to interpret this interesting nonlinear spectrum. Note that the horizontal frequency axis is centered at the peak of the spectrum where the frequency is taken to be zero. There are two kinds of IST spectrum. The first kind of spectrum has simple sine waves (or at most low amplitude Stokes wave components) that are shown connecting to the frequency axis by a line, a "spine". These are the low lying components to the right and left of the spectrum and one can think of them as being like ordinary linear Fourier components. The other kind of spectrum is totally new and consists of unstable wave packets. These consist of double points connected by a spine. When the double points are degenerate no spine can be seen because the two points lie almost on top of each other. In other cases the spines can be seen clearly connecting the double points. In any event any isolated cross, or two crosses

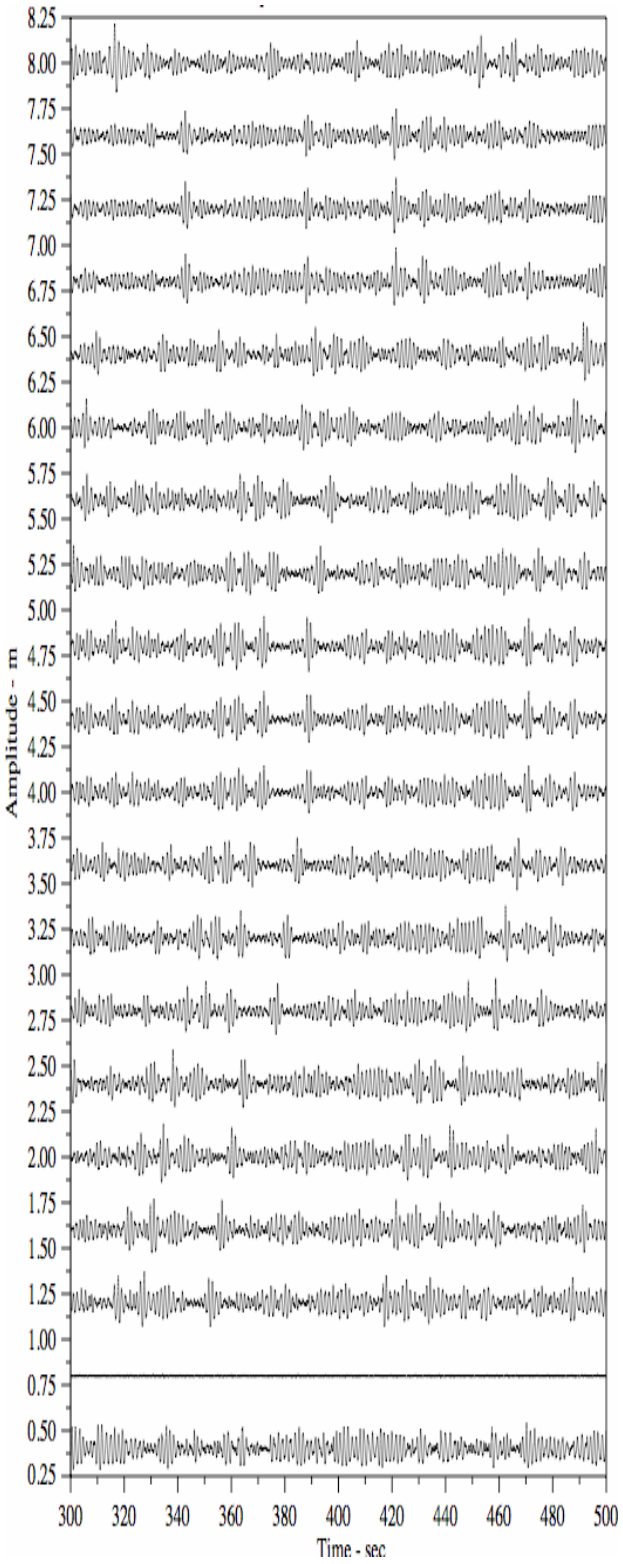


connected by a spine are unstable packet modes. Crosses connected to the frequency axis by a spine are quasi-linear modes (like linear Fourier components). Thus all of the crosses in Figure 15 in the upper part of the picture are unstable packets; there are 13 of them, the larger of which are candidates for extreme waves at some point during their nonlinear evolution.

←**Figure 10.** A 200-sec section of a random wave experiment conducted at Marintek. We used the value $\gamma = 6$ for the JONSWAP power spectrum.

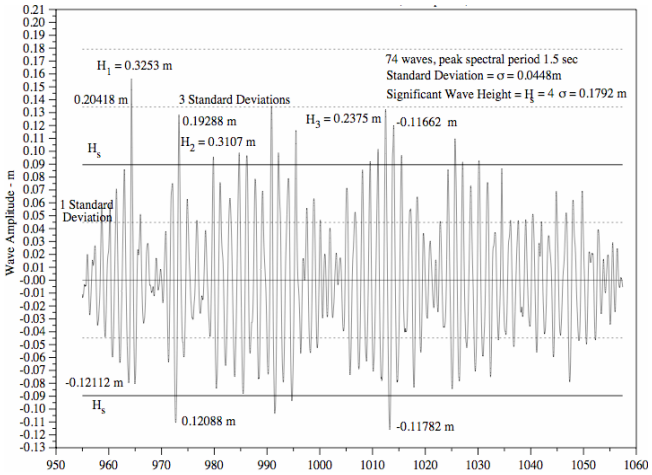


**Figure 11.** A 4096 point time series from Probe 1 at 10 m from the wave maker.

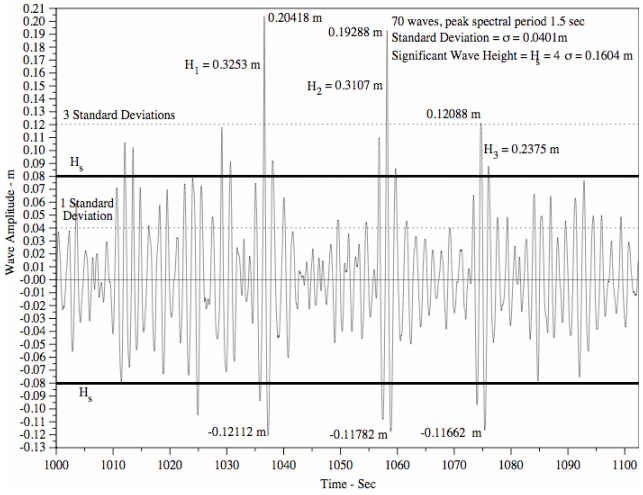


**Figure 12.** A 4096 point time series from Probe 8 at 70 m from the wave maker. Three extreme waves have amplitudes that are greater than three standard deviations. Two of the waves are greater than twice the significant wave height.

To properly interpret the IST spectrum of Figure 15 we compare to the linear Fourier spectrum on the same scale, see Figure 16. All of the modes are stable and consist of sine waves. How can the nonlinear spectrum in Figure 15 have so many unstable wave packets? Because, simply put, they have robbed energy from the linear Fourier modes.

We finally compare the heights of the largest ob-

served packets in the time series of Figure 12 with inverse scattering theory using Figure 15 and Eq. (12). The results are shown in Figure 17. The theory of Eq. (12) is shown as a solid line. The wave heights measured from Figure 14 (which has been filtered for the Stokes effect) are shown as solid squares. The wave heights measured from Figure 12 (no filtering for the Stokes effect) are shown as open squares. One does not expect perfect agreement between theory and experiment because the measurements at Probe 8 give the packet heights only at one spatial location. Since the packets are unstable their amplitudes are undergoing considerable space/time dynamics and we cannot expect that they will all be at their maximum heights at *any* spatial location. The results of Figure 17 show the observed wave heights to fall below their maximum theoretical heights, an expected result.

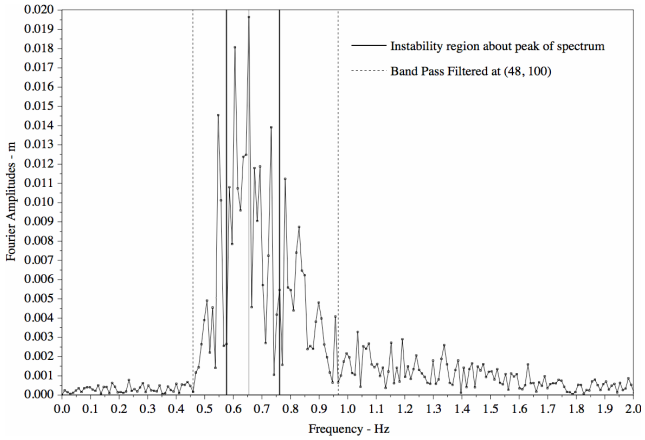


**Figure 13.** Fourier transform of time series at Probe 8 in Figure 12. The location of the band pass filter that removes the Stokes contribution is also shown.

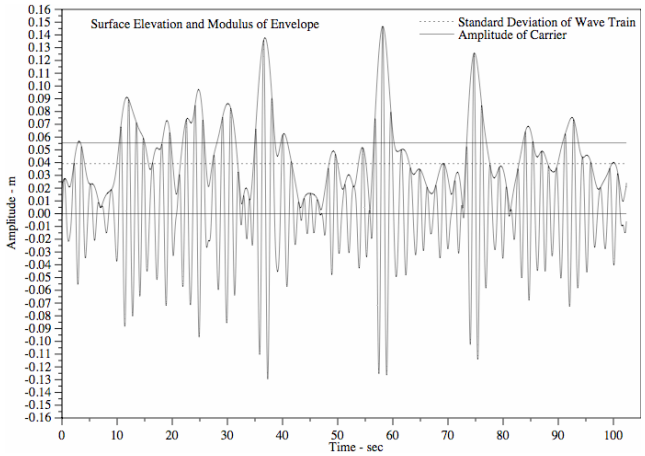


**Figure 14.** Application of the Hilbert transform to the time series at Probe 8 in Figure to determine the modulus of the envelope of the wave train. This step also includes the filtering operation discussed in Figure 13.

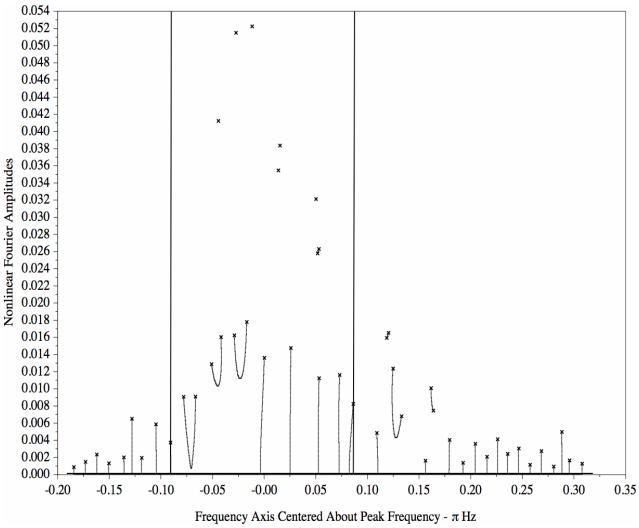


**Figure 15**. Inverse scattering transform spectrum of the time series at Probe 8 in Figure 12. Eigenvalue pairs that are in the upper part of the graph correspond to large unstable wave packets. The carrier height is at 0.0566 m.

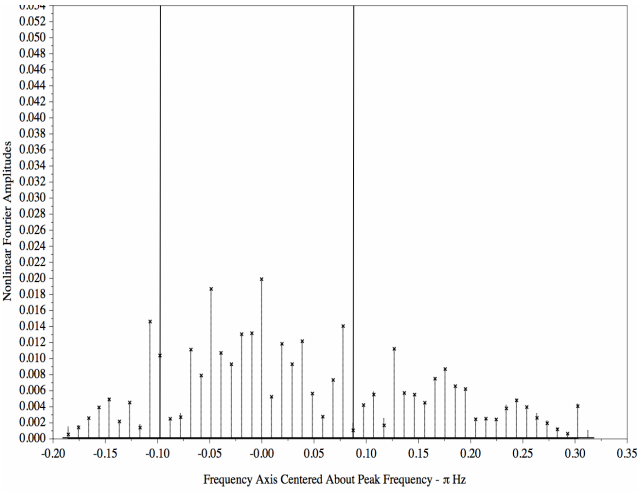


**Figure 16.** Linear Fourier spectrum of the time series at Probe 8 in Figure 12. The scale is the same as the IST spectrum in Figure 15, so that comparison of the two can be made. The bounds of the linear estimate of unstable modes are indicated by the vertical lines.

It is interesting to note that the Benjamin-Feir parameter, as computed by Eq. (21), is $I_{BF} = 9.79$. This result is based upon linearized modulation theory and should be compared to the number of unstable packets in Figure 15, namely, 13. Complete inverse scattering theory contains the full NLS spectrum, including *large amplitude modulations*. In the present case the number of fully nonlinear modes is 13, larger than the 9 modes estimated by the BF parameter.

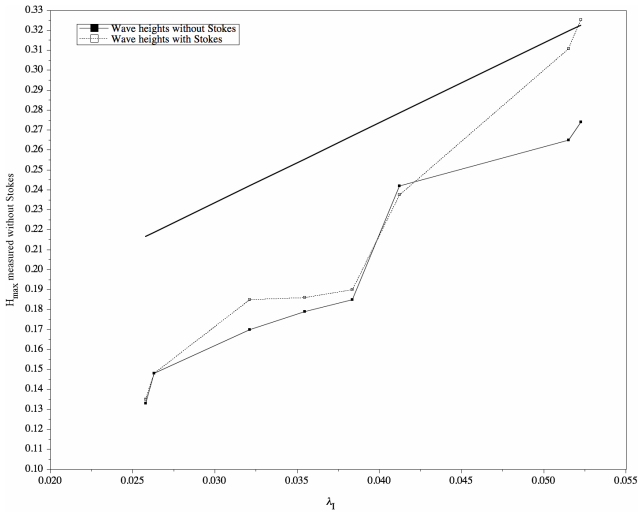


**Figure 17.** The largest packet heights predicted by theory (solid line) to the actual packet heights measured from Figures 12 (with Stokes contribution) and 13 (Stokes contribution filtered out).

## 8. Summary and discussion

We have used the periodic inverse scattering transform to study the nonlinear dynamics of deep-water wave trains, both theoretically and experimentally. Experimentally we have used IST as a time series analysis tool to enhance our understanding of measured wave trains in the wave tank facility at Marintek, Trondheim, Norway. We have discussed how deep water wave trains have two kinds of spectrum, namely, a near linear component and a separate component of unstable wave packets. These packets are discrete components of the IST spectrum, they have their own nonlinear space/time dynamics and also nonlinearly interact with one another and the near-linear background sea state.

**Acknowledgments**. This work is supported by the Office of Naval Research. This work was also supported by the European Community, a Cofin Grant and two MURST (Ministero Università e Ricerca Scientifica Tecnologica) grants from Italy.

## References

Ablowitz, M. J. and H. Segur, *Solitons and the Inverse Scattering Transform* (SIAM, Philadelphia), 1981.

Forristall, G.Z., Wave crest distributions: Observations and second order theory, *J. Phys. Oceanogr.*, 30, 1931–1943.

Graveson, A, "Design and Operation for Abnormal Conditions," seminar at conference of Royal Institution of Naval Architects, MarineLog.com, 28 January, 2005.

Its, A. R., and V. B. Matveev, The periodic Korteweg-deVries equation, *Func. Anal. Appl.,* 9(1), 67, 1975.

Janssen, P. A. E. M., Nonlinear Four-Wave Interactions and Freak Waves, *J. Physical Oceanogr. 33*, 863–883, 2003.

Korteweg, D. J. and G. deVries, On the change of form of long waves advancing in a rectangular canal, and on a new type of long stationary waves*, Philos. Mag. Ser., Vol. 5*(39), 422-443, 1895.

Kotljarov, V. P. and A. R. Its*, Dopovidi Akad. Nauk. UkRSR., Ser. A, Vol. 11*, 965-968 (in Ukranian), 1976.

Osborne, A. R., M. Onorato, and M. Serio, The nonlinear dynamics of rogue waves and holes in deep-water gravity wave trains, *Phys. Lett. A* 275, 386, 2000.

Osborne, A. R., Nonlinear Ocean Waves and the Inverse Scattering Transform, In *Scattering*, ed. by R. Pike and P. Sabatier, Academic Press, 2002.

Tayfun, M. A., Narrow-Band Nonlinear Sea Waves. *J. Geophys. Res*., 85(C3), 1548–1552, 1980. Tracy, E. R. and Chen, H. H. ,1988, *Phys. Rev. A* 37, 815.

Whitham, G. B. 1974, Linear and Nonlinear Waves. Wiley, New York.

Zakharov, V. E. 1968, *J. Appl. Mech. Tech. Phys*. 2, 190.